JOURNAL OF THEORETICAL AND APPLIED MECHANICS
62, 4, pp. 667-681, Warsaw 2024
https://doi.org/10.15632/jtam-pl/193256

DYNAMIC RESPONSE OF SATURATED FROZEN SOIL FOUNDATION UNDER UNDERLYING BEDROCK TO HARMONIC LOAD

Huaiyuan Chen

School of Civil Engineering, Qinghai University, Xining810016, China

Qiang Ma

School of Civil Engineering, Qinghai University, Xining810016, China, and

Qinghai Provincial Key Laboratory of Energy-saving Building Materials and Engineering Safety, Xining, China

e-mail: maqiang0104@163.com

This study aims to provide a theoretical basis for engineering construction in alpine frozen soil area, simplify the soil medium of the site in alpine permafrost region to saturated permafrost, and expand the elastic foundation and saturated ground foundation to better reflect the dynamic response problem of permafrost st site in alpine region. Based on the theory of solid porous media with pores, a physical model of dynamic response of saturated frozen soil foundation with underlying bedrock under vertical harmonic load is established, and the effects of temperature, porosity, cementation parameters, load frequency and contact parameters on the dynamic response are analyzed.

Keywords: soil medium, saturated frozen soil foundation, dynamic response

1. Introduction

China is the third largest frozen soil country in the world. Frozen soil is mainly distributed in China's western high-altitude and cold regions. With the implementation of the national western development strategy and the "One Belt, One Road" strategy, there are many infrastructure projects under construction which are proposed to be implemented in the western high-altitude and high-cold areas. Because the soil layer in the western high altitude and cold area is frozen chiefly soil, the mechanical properties of frozen soil are very different from those of unfrozen soil. Therefore, in order to ensure stability as well as safety of engineering buildings in the permafrost region, the research on the dynamic response of permafrost needs to be carried out urgently.

Since the first study of single-phase elastic half-space dynamics by Lamb (1904) in 1904, more and more scholars (Ai *et al.*, 2018; Liang *et al.*, 2020) have gradually improved the theoretical study of the dynamic response of single-phase elastic foundations. However, it is not practical to analyze the soil by simply assuming it to be single-phase elastic, and when the single-phase soil is filled with water, it becomes two-phase saturated soil. Biot (1956; 1962) was the first to study the dynamic response of saturated soil foundation, and put forward the fluctuation equation of saturated soil. Based on Biot's theory, Zhou *et al.* (2013) obtained numerical solutions for the displacement and stress integrals of soil particles and pore water in saturated soils when simple harmonic loads were applied to the surface of the saturated soil foundation. Xu *et al.* (2009) further considered the layered nature of the soil, and used the transfer matrix method and Hankel transform to study the dynamic response of a layered saturated soil foundation when a horizontal simple harmonic load was applied to the surface of the foundation, and found that the layered nature of the soil had a significant effect on the dynamic response of the foundation. Liu *et al.* (2022) investigated the dynamic response of a layered transverse

isotropic saturated land base under two-dimensional moving loads under permeable and impermeable conditions on the surface using Fourier series expansion and dual variable and position methods. However, soils in nature are usually unsaturated soils, which consist of three phases: gas phase, liquid phase and soil particle phase, and the influence of gas phase in unsaturated soils on the dynamic response should not be neglected. Considering the coupling effect of the three phases of unsaturated soils, Xu (2010) and Xu *et al.* (2011) obtained the fluctuation equation of unsaturated soils by using Bishop's effective stress equation combined with the V-G model of capillary pressure function, and investigated the dynamic response of unsaturated semi-space surfaces under arbitrary loading. Shi *et al.* (2021; 2022) investigated the dynamic response of semi-space unsaturated soil foundations under simple harmonic loads under different boundary conditions by utilizing the Fourier transform. Ma *et al.* (2023a) developed a layered foundation model and analyzed and discussed the dynamic response of three types of layered unsaturated foundations, homogeneous soil, hard interbedded and soft interbedded, under moving loads using coordinate transformations and the transfer and reflection matrix method. Ma *et al.* (2023b) investigated the dynamic response of different types of loads on transversely isotropic multilayered unsaturated and ground foundations in a three-dimensional column coordinate system using the Laplace-Hankel transform.

The above studies on the foundation dynamic response mostly regard foundation soil as single-phase elastic soil, two-phase saturated soil and three-phase unsaturated soil, but in the high-latitude and high-altitude region of western China, the site soil medium is mostly permafrost, and many projects in the western region involve permafrost, and the dynamic response of the permafrost is very different from that of the unfrozen soil due to the existence of the ice phase. Therefore, on the basis of the above research, this paper simplifies the frozen soil into saturated frozen soil, establishes the two-dimensional saturated frozen soil foundation power control equation under a simple harmonic load based on the theory of porous solid porous medium, and obtains the answer to the question of the power response of saturated frozen soil foundation in the frequency domain by using the Fourier integral transform, the principle of Helmholtz vector decomposition and combining with the boundary conditions. The effects of temperature, porosity, cementation parameters, and loading frequency on the dynamic response of a two-dimensional saturated frozen soil foundation are analyzed and discussed through numerical examples.

2. Mechanical model and governing equations

2.1. Mechanical model

Considering a saturated frozen soil foundation with finite thickness, the surface action has a vertical strip harmonic load, as shown in Fig. 1, where H is the layer thickness, q_0 is the linear load acting on the surface of the foundation, l is the half of the linear load length, q is the load amplitude, $q = q_0/(2\pi)$, and ω is the circular frequency of the load vibration. Assuming that the surface is permeable and the bottom bedrock is impermeable, the coordinate axis shown in the diagram is established, and the coordinate origin is placed on the surface of the foundation, that is, the surface of the foundation $z = 0$.

2.2. Governing equations

According to the definition of Zhou and Lai (2011), ice is formed in pores and coexists with liquid water in thepores. Therefore, saturated frozen soil can be regarded as a three-phase porous medium composed of soil particle phase, pore liquid water phase, and pore ice phase, that is, solid phase, liquid phase, and ice phase. The volume fraction of each phase is expressed as follows

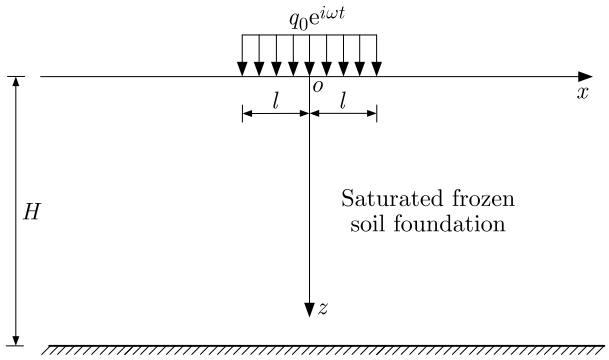

Fig. 1. A schematic diagram of the harmonic load acting on a two-dimensional saturated frozen soil foundation

$$\phi_S = 1 - \phi \qquad \phi_F = \phi S_r \qquad \phi_I = \phi(1 - S_r) \tag{2.1}$$

where S_r denotes the saturation level of pore liquid water, ϕ denotes the porosity of porous media; the subscripts S, F and I denote the volume fraction of soil particles, pore liquid water, and pore ice in saturated frozen soil, respectively.

Under a harmonic load, the stress and displacement of each phase in saturated frozen soil can be expressed as follows

$$G(x, z, t) = G(x, z)^* \mathrm{e}^{\mathrm{i}\omega t} \tag{2.2}$$

where i is an imaginary unit, ω is the frequency of load circle; for the convenience of representation, the superscript $*$ in the following text is omitted.

The governing equation for saturated frozen soil can be derived based on the theory presented by Leclaire *et al.* (1994, 1995) and further developed by Carcione *et al.* (2000, 2003), Carcione and Seriani (2001)

$$\begin{aligned}
&\rho_{11}\ddot{\mathbf{u}}^S + \rho_{12}\ddot{\mathbf{u}}^F + \rho_{13}\ddot{\mathbf{u}}^I = R_{11}\nabla(\nabla\cdot\mathbf{u}^S) + R_{12}\nabla(\nabla\cdot\mathbf{u}^F) + R_{13}\nabla(\nabla\cdot\mathbf{u}^I)\\
&\quad - \mu_{11}\nabla\times\nabla\times\mathbf{u}^S - \mu_{13}\nabla\times\nabla\times\mathbf{u}^I - (b_{12}+b_{13})\dot{\mathbf{u}}^S + b_{12}\dot{\mathbf{u}}^F + b_{13}\dot{\mathbf{u}}^I\\
&\rho_{12}\ddot{\mathbf{u}}^S + \rho_{22}\ddot{\mathbf{u}}^F + \rho_{23}\ddot{\mathbf{u}}^I = R_{12}\nabla(\nabla\cdot\mathbf{u}^S) + R_{22}\nabla(\nabla\cdot\mathbf{u}^F) + R_{23}\nabla(\nabla\cdot\mathbf{u}^I)\\
&\quad + b_{12}\dot{\mathbf{u}}^S - (b_{12}+b_{23})\dot{\mathbf{u}}^F + b_{23}\dot{\mathbf{u}}^I\\
&\rho_{13}\ddot{\mathbf{u}}^S + \rho_{23}\ddot{\mathbf{u}}^F + \rho_{33}\ddot{\mathbf{u}}^I = R_{13}\nabla(\nabla\cdot\mathbf{u}^S) + R_{23}\nabla(\nabla\cdot\mathbf{u}^F) + R_{33}\nabla(\nabla\cdot\mathbf{u}^I)\\
&\quad - \mu_{13}\nabla\times\nabla\times\mathbf{u}^S - \mu_{33}\nabla\times\nabla\times\mathbf{u}^I + b_{13}\dot{\mathbf{u}}^S + b_{23}\dot{\mathbf{u}}^F - (b_{13}+b_{23})\dot{\mathbf{u}}^I
\end{aligned} \tag{2.3}$$

where ρ_{ij} $(i = 1, 2, 3;\ j = 1, 2, 3)$ denote the coupling inertia coefficients between each phase; $\mathbf{u}^S$, $\mathbf{u}^F$ and $\mathbf{u}^I$ denote the displacement vectors of soil particles, pore liquid water, and pore ice in the saturated frozen soil medium, respectively. b_{12}, b_{23} and b_{13} are viscosity parameters; R_{ij} $(i = 1, 2, 3;\ j = 1, 2, 3)$ and μ_{11}, μ_{13}, μ_{33} are stiffness parameters. The coefficients of ρ_{ij}, R_{ij}, μ_{11}, μ_{13}, μ_{33}, b_{12}, b_{23}, b_{13}, etc. are detailed in Qiu *et al.* (2018) literature. The symbols $(\cdot)$, $(\cdot\cdot)$ denote the first and second derivatives with respect to time, respectively; ∇^2 is the Laplacian operator in a Cartesian coordinate system.

The stress-strain relationship in the saturated permafrost medium is as follows

$$\begin{aligned}
\sigma_{ij}^S &= (K_1\theta_S + C_{12}\theta_F + C_{13}\theta_I)\delta_{ij} + 2\mu_{11}d_{ij}^S + \mu_{13}d_{ij}^I\\
\sigma^F &= C_{12}\theta_S + K_2\theta_F + C_{23}\theta_I\\
\sigma_{ij}^I &= (C_{13}\theta_S + C_{23}\theta_F + K_3\theta_I)\delta_{ij} + 2\mu_{33}d_{ij}^I + \mu_{13}d_{ij}^S
\end{aligned} \tag{2.4}$$

and

$$
\begin{aligned}
&C_{12}=(1-c_1)\phi_S\phi_F K_{av} \qquad C_{13}=(1-c_1)(1-c_3)\phi_S\phi_I K_{av}\\
&C_{23}=(1-c_3)\phi_I\phi_F K_{av}\\
&K_1=[(1-c_1)\phi_S]^2K_{av}+K_{sm} \qquad K_2=\phi_F^2K_{av} \qquad K_3=[(1-c_3)\phi_I]^2K_{av}+K_{im}\\
&\theta_S=u^S_{i,i} \qquad \theta_F=u^F_{i,i} \qquad \theta_I=u^I_{i,i}\\
&d^S_{ij}=\varepsilon^S_{ij}-\frac{1}{3}\theta_S\delta_{ij} \qquad d^I_{ij}=\varepsilon^I_{ij}-\frac{1}{3}\theta_I\delta_{ij} \qquad \varepsilon^S_{ij}=\frac{1}{2}(u^S_{i,j}+u^S_{j,i})\\
&\varepsilon^I_{ij}=\frac{1}{2}(u^I_{i,j}+u^I_{j,i})
\end{aligned}
\tag{2.5}
$$

where σ^S_{ij}, σ^F, σ^I_{ij} denote the stress components acting on the solid phase, liquid phase, and ice phase, respectively; K_1, K_2 and K_3 are bulk moduli of elasticity; C_{12}, C_{13} and C_{23} are the bulk modulus between the three phases. δ_{ij} is the Kronecker symbol; ε^a_{ij}, d^a_{ij} and θ_a denote the body strain, bias strain, and strain of the a ($a=S,F,I$) phase, respectively. The coefficients of c_1, c_3, K_{av}, K_{im}, K_{sm}, etc. are detailed in Qiu *et al.* (2018).

According to Zhou (2020), among the parameters involved in the governing equations of saturated frozen soil, porosity, and ice content are considered to be significant factors that influence the characteristics of the soil. Leclaire *et al.* (1994) used the normal distribution of pores to describe the ice content and considered that at a certain temperature, when the pore is less than a certain scale, the water in the pore will not freeze, and the water in the pore larger than this pore diameter will freeze completely. Therefore, the relationship between temperature and pore ice content is calculated as follows

$$
\phi_F=(1-\phi_S)A\int_0^{r_0/\ln(T_0/T_{k0})}\exp\Big[-\frac{(r-r_{av})^2}{2\Delta r^2}\Big]\,dr \tag{2.6}
$$

By normalizing the Gaussian probability function from $r=0\to\infty$, the expression of unfrozen water content used in this paper can be expressed as follows

$$
\phi_F=(1-\phi_S)\frac{\operatorname{erf}(\zeta)+\operatorname{erf}(\eta)}{1+\operatorname{erf}(\eta)} \qquad \zeta=\frac{r_0/\ln(T_0/T_{k0})}{\sqrt{2}\Delta r}-\eta \qquad \eta=\frac{r_{av}}{\sqrt{2}\Delta r} \tag{2.7}
$$

where r_{av} is the average pore radius; Δr is the standard deviation of pore radius; $r_0=0.228\,\mathrm{nm}$, $T_{k0}=T+T_0$, T_{k0}, T_0, T all indicate temperature, T_{k0}, T_0 in Kelvin, $T_0=273.15\,\mathrm{K}$, T in Celsius. The parameters η, ζ are explained in detail in Carcione and Seriani (2001).

Substituting Eq. (2.2) into Eqs. (2.3), we can get the following

$$
\begin{aligned}
&a_{11}\mathbf{u}^S+a_{12}\mathbf{u}^F+a_{13}\mathbf{u}^I=R_{11}\nabla(\nabla\cdot\mathbf{u}^S)+R_{12}\nabla(\nabla\cdot\mathbf{u}^F)+R_{13}\nabla(\nabla\cdot\mathbf{u}^I)\\
&\quad-\mu_{11}\nabla\times\nabla\times\mathbf{u}^S-\mu_{13}\nabla\times\nabla\times\mathbf{u}^I\\
&a_{12}\mathbf{u}^S+a_{22}\mathbf{u}^F+a_{23}\mathbf{u}^I=R_{12}\nabla(\nabla\cdot\mathbf{u}^S)+R_{22}\nabla(\nabla\cdot\mathbf{u}^F)+R_{23}\nabla(\nabla\cdot\mathbf{u}^I)\\
&a_{13}\mathbf{u}^S+a_{23}\mathbf{u}^F+a_{33}\mathbf{u}^I=R_{13}\nabla(\nabla\cdot\mathbf{u}^S)+R_{23}\nabla(\nabla\cdot\mathbf{u}^F)+R_{33}\nabla(\nabla\cdot\mathbf{u}^I)\\
&\quad-\mu_{13}\nabla\times\nabla\times\mathbf{u}^S-\mu_{33}\nabla\times\nabla\times\mathbf{u}^I
\end{aligned}
\tag{2.8}
$$

where $a_{11}=-\rho_{11}\omega^2+(b_{12}+b_{13})\mathrm{i}\omega$, $a_{12}=-\rho_{12}\omega^2-b_{12}\mathrm{i}\omega$, $a_{13}=-\rho_{13}\omega^2-b_{13}\mathrm{i}\omega$, $a_{22}=-\rho_{22}\omega^2+(b_{12}+b_{23})\mathrm{i}\omega$, $a_{23}=-\rho_{23}\omega^2-b_{23}\mathrm{i}\omega$, $a_{33}=-\rho_{33}\omega^2+(b_{13}+b_{23})\mathrm{i}\omega$.

The displacement vector of each phase can be expressed by the Helmholtz vector decomposition theorem as

$$
u^a=\nabla\varphi_a+\nabla\times\psi_a \qquad \nabla\cdot\psi_a=0 \qquad a=S,F,I \tag{2.9}
$$

where φ_a and ψ_a are the three-phase medium scalar and vector potential functions, respectively.

Substituting Eq. (2.9) into Eqs. (2.8), we can get

$$\begin{aligned} a_{11}\varphi_S + a_{12}\varphi_F + a_{13}\varphi_I &= R_{11}\nabla^2\varphi_S + R_{12}\nabla^2\varphi_F + R_{13}\nabla^2\varphi_I \\ a_{12}\varphi_S + a_{22}\varphi_F + a_{23}\varphi_I &= R_{12}\nabla^2\varphi_S + R_{22}\nabla^2\varphi_F + R_{23}\nabla^2\varphi_I \\ a_{13}\varphi_S + a_{23}\varphi_F + a_{33}\varphi_I &= R_{13}\nabla^2\varphi_S + R_{23}\nabla^2\varphi_F + R_{33}\nabla^2\varphi_I \end{aligned} \tag{2.10}$$

$$\begin{aligned} &a_{11}\psi_S + a_{12}\psi_F + a_{13}\psi_I = \mu_{11}\nabla^2\psi_S + \mu_{13}\nabla^2\psi_I \\ &a_{12}\psi_S + a_{22}\psi_F + a_{23}\psi_I = 0 \qquad a_{13}\psi_S + a_{23}\psi_F + a_{33}\psi_I = \mu_{13}\nabla^2\psi_S + \mu_{33}\nabla^2\psi_I \end{aligned} \tag{2.11}$$

3. The solution of the potential function

The above governing equations can be transformed into ordinary differential equations, which are easy to solve by the Fourier transform of the horizontal coordinate x. The Fourier transform of the function $f(x,z)$ is as follows

$$\widetilde{f}(\xi,z) = \int_{-\infty}^{\infty} f(x,z)\mathrm{e}^{-\mathrm{i}\xi x}\,dx \tag{3.1}$$

where ξ is the Fourier transform parameter, the superscript $\widetilde{(\cdot)}$ denotes the Fourier transform of the space coordinate x.

The Fourier transform of Eqs. (2.10) can be obtained

$$\begin{aligned} &R_{11}\frac{d^2\widetilde{\varphi}_S}{dz^2} + A_{11}\widetilde{\varphi}_S + R_{12}\frac{d^2\widetilde{\varphi}_F}{dz^2} + A_{12}\widetilde{\varphi}_F + R_{13}\frac{d^2\widetilde{\varphi}_I}{dz^2} + A_{13}\widetilde{\varphi}_I = 0 \\ &R_{12}\frac{d^2\widetilde{\varphi}_S}{dz^2} + A_{12}\widetilde{\varphi}_S + R_{22}\frac{d^2}{\widetilde{\varphi}_F}dz^2 + A_{22}\widetilde{\varphi}_F + R_{23}\frac{d^2\widetilde{\varphi}_I}{dz^2} + A_{23}\widetilde{\varphi}_I = 0 \\ &R_{13}\frac{d^2\widetilde{\varphi}_S}{dz^2} + A_{13}\widetilde{\varphi}_S + R_{23}\frac{d^2\widetilde{\varphi}_F}{dz^2} + A_{23}\widetilde{\varphi}_F + R_{33}\frac{d^2\widetilde{\varphi}_I}{dz^2} + A_{33}\widetilde{\varphi}_I = 0 \end{aligned} \tag{3.2}$$

where $A_{11} = -a_{11} - \xi^2 R_{11}$, $A_{12} = -a_{12} - \xi^2 R_{12}$, $A_{13} = -a_{13} - \xi^2 R_{13}$, $A_{22} = -a_{22} - \xi^2 R_{22}$, $A_{23} = -a_{23} - \xi^2 R_{23}$, $A_{33} = -a_{33} - \xi^2 R_{33}$.

The solution of Eqs. (3.2) is assumed as follows

$$[\widetilde{\varphi}_S, \widetilde{\varphi}_F, \widetilde{\varphi}_I]^{\mathrm{T}} = [c^S, c^F, c^I]^{\mathrm{T}} \exp(\lambda z) \tag{3.3}$$

By substituting Eq. (3.3) into Eqs. (3.2), we obtain the following system of linear equations

$$\begin{bmatrix} \lambda^2 R_{13} + A_{13} & \lambda^2 R_{12} + A_{12} & \lambda^2 R_{11} + A_{11} \\ \lambda^2 R_{23} + A_{23} & \lambda^2 R_{22} + A_{22} & \lambda^2 R_{12} + A_{12} \\ \lambda^2 R_{33} + A_{33} & \lambda^2 R_{23} + A_{23} & \lambda^2 R_{13} + A_{13} \end{bmatrix} \begin{bmatrix} c^I \\ c^F \\ c^S \end{bmatrix} = 0 \tag{3.4}$$

When the coefficient matrix determinant is zero, Eq. (3.4) has a non-zero solution, that is

$$\beta_1\lambda^6 + \beta_2\lambda^4 + \beta_3\lambda^2 + \beta_4 = 0 \tag{3.5}$$

where

$$\begin{aligned} \beta_1 &= -R_{11}R_{22}R_{33} + R_{11}R_{23}^2 + R_{12}^2R_{33} - 2R_{12}R_{13}R_{23} + R_{13}^2R_{22} \\ \beta_2 &= -A_{11}R_{22}R_{33} + A_{11}R_{23}^2 + 2A_{12}R_{12}R_{33} - 2A_{12}R_{13}R_{23} - 2A_{13}R_{12}R_{23} + 2A_{13}R_{13}R_{22} \\ &\quad - A_{22}R_{11}R_{33} + A_{22}R_{13}^2 + 2A_{23}R_{11}R_{23} - 2A_{23}R_{12}R_{13} - A_{33}R_{11}R_{22} + A_{33}R_{12}^2 \\ \beta_3 &= -A_{11}A_{22}R_{33} + 2A_{11}A_{23}R_{22} - A_{11}A_{33}R_{22} + A_{12}^2R_{33} - 2A_{12}A_{13}R_{23} - 2A_{12}A_{23}R_{13} \\ &\quad + 2A_{12}A_{33}R_{12} + A_{13}^2R_{22} + 2A_{13}A_{22}R_{13} - 2A_{13}A_{23}R_{12} - A_{22}A_{33}R_{11} + A_{23}^2R_{11} \\ \beta_4 &= -A_{11}A_{22}A_{33} + A_{11}A_{23}^2 + A_{12}^2A_{33} - 2A_{12}A_{13}A_{23} + A_{13}^2A_{22} \end{aligned}$$

The roots of Eq. (2.5), denoted as $\pm\lambda_n$ $(n = 1, 2, 3)$, can be obtained by solving the following equation

$$\lambda_n = \sqrt{d_n}(\mathrm{Re}[\lambda_n] \geqslant 0 \qquad n = 1, 2, 3 \tag{3.6}$$

where d_n are determined by the equation $\beta_1 d_n^3 + \beta_2 d_n^2 + \beta_3 d_n + \beta_4 = 0$.

The general solution of the system of Eqs. (3.2) can be obtained as

$$\begin{aligned} &\widetilde{\varphi}_S = \sum_{n=1}^{3}(D_n \mathrm{e}^{-\lambda_n z} + E_n \mathrm{e}^{\lambda_n z}) \qquad \widetilde{\varphi}_F = \sum_{n=1}^{3}\delta_{pn}^F(D_n \mathrm{e}^{-\lambda_n z} + E_n \mathrm{e}^{\lambda_n z}) \\ &\widetilde{\varphi}_I = \sum_{n=1}^{3}\delta_{pn}^I(D_n \mathrm{e}^{-\lambda_n z} + E_n \mathrm{e}^{\lambda_n z}) \end{aligned} \tag{3.7}$$

where D_i and E_i $(i = 1, 2, 3)$ are undetermined coefficients

$$\begin{aligned} \delta_{pn}^F &= \frac{(R_{11}R_{23} - R_{12}R_{13})d_n^2 + (A_{11}R_{23} - A_{12}R_{13} - A_{13}R_{12} + A_{23}R_{11})d_n + A_{11}A_{23} - A_{12}A_{13}}{(-R_{12}R_{23} + R_{13}R_{22})d_n^2 + (-A_{12}R_{23} + A_{13}R_{22} + A_{22}R_{13} - A_{23}R_{12})d_n - A_{12}A_{23} + A_{13}A_{22}} \\ \delta_{pn}^I &= \frac{(-R_{11}R_{22} + R_{12}^2)d_n^2 + (-A_{11}R_{22} + 2A_{12}R_{12} - A_{22}R_{11})d_n - A_{11}A_{22} + A_{12}^2}{(-R_{12}R_{23} + R_{13}R_{22})d_n^2 + (-A_{12}R_{23} + A_{13}R_{22} + A_{22}R_{13} - A_{23}R_{12})d_n - A_{12}A_{23} + A_{13}A_{22}} \end{aligned}$$

The Fourier transform of Eqs. (2.11) can be obtained

$$\begin{aligned} &\mu_{11}\frac{d^2\widetilde{\psi}_S}{dz^2} + B_{11}\widetilde{\psi}_S + B_{12}\widetilde{\psi}_F + \mu_{13}\frac{d^2\widetilde{\psi}_I}{dz^2} + B_{13}\widetilde{\psi}_I = 0 \\ &B_{21}\widetilde{\psi}_S + B_{22}\widetilde{\psi}_F + B_{23}\widetilde{\psi}_I = 0 \\ &\mu_{13}\frac{d^2\widetilde{\psi}_S}{dz^2} + B_{31}\widetilde{\psi}_S + B_{32}\widetilde{\psi}_F + \mu_{33}\frac{d^2\widetilde{\psi}_I}{dz^2} + B_{33}\widetilde{\psi}_I = 0 \end{aligned} \tag{3.8}$$

where $B_{11} = -a_{11} - \xi^2\mu_{11}$, $B_{12} = -a_{12}$, $B_{13} = -a_{13} - \xi^2\mu_{13}$, $B_{21} = a_{12}$, $B_{22} = a_{22}$, $B_{23} = a_{23}$, $B_{31} = -a_{13} - \xi^2\mu_{13}$, $B_{32} = -a_{23}$, $B_{33} = -a_{33} - \xi^2\mu_{33}$.

The solution of Eqs. (3.8) is assumed as follows

$$[\widetilde{\psi}_S, \widetilde{\psi}_F, \widetilde{\psi}_I]^{\mathrm{T}} = [h^S, h^F, h^I]^{\mathrm{T}} \exp(rz) \tag{3.9}$$

Substituting Eq. (3.9) into Eqs. (3.8), the linear equations are obtained

$$\begin{bmatrix} \mu_{13}r^2 + B_{13} & B_{12} & \mu_{11}r^2 + B_{11} \\ B_{23} & B_{22} & B_{21} \\ \mu_{33}r^2 + B_{33} & B_{32} & \mu_{13}r^2 + B_{31} \end{bmatrix} \begin{bmatrix} h^I \\ h^F \\ h^S \end{bmatrix} = 0 \tag{3.10}$$

When the coefficient matrix determinant is zero, Eq. (9.10) has a non-zero solution, that is

$$\beta_5 r^4 + \beta_6 r^2 + \beta_7 = 0 \tag{3.11}$$

where

$$\begin{aligned} \beta_5 &= -\mu_{11}\mu_{33}B_{22} + \mu_{13}^2 B_{22} \\ \beta_6 &= -\mu_{11}B_{22}B_{33} + \mu_{11}B_{23}B_{32} - \mu_{13}B_{12}B_{23} + \mu_{13}B_{13}B_{22} - \mu_{13}B_{21}B_{32} + \mu_{13}B_{22}B_{31} \\ &\quad - \mu_{33}B_{11}B_{22} + \mu_{33}B_{12}B_{21} \\ \beta_7 &= -B_{11}B_{22}B_{33} + B_{11}B_{23}B_{32} + B_{12}B_{21}B_{33} - B_{12}B_{23}B_{31} - B_{13}B_{21}B_{32} + B_{13}B_{22}B_{31} \end{aligned}$$

The roots of Eq. (3.11), denoted as $\pm r_n$ $(n = 1, 2)$, can be obtained by solving the following equation

$$r_n = \sqrt{t_n}(\mathrm{Re}[r_n] \geqslant 0 \qquad n = 1, 2 \tag{3.12}$$

where t_n are determined from the equation $\beta_5 t_n^2 + \beta_6 t_n + \beta_7 = 0$.

The general solution of the system of Eqs. (3.8) can be obtained as

$$\begin{aligned} &\widetilde{\psi}_S = \sum_{n=1}^{2}(M_n \mathrm{e}^{-r_n z} + N_n \mathrm{e}^{r_n z}) \qquad \widetilde{\psi}_F = \sum_{n=1}^{2}\delta_{sn}^F(M_n \mathrm{e}^{-r_n z} + N_n \mathrm{e}^{r_n z}) \\ &\widetilde{\psi}_I = \sum_{n=1}^{2}\delta_{sn}^I(M_n \mathrm{e}^{-r_n z} + N_n \mathrm{e}^{r_n z}) \end{aligned} \tag{3.13}$$

where M_1, M_2, N_1 and N_2 are undetermined coefficients

$$\delta_{sn}^F = \frac{(\mu_{11}t_n + B_{11})B_{23} - B_{21}(\mu_{13}t_n + B_{13})}{-B_{23}B_{12} + B_{22}\mu_{13}t_n + B_{13})} \qquad \delta_{sn}^I = \frac{(-\mu_{11}t_n + B_{11})B_{22} - B_{12}B_{21}}{-B_{23}B_{12} + B_{22}(\mu_{13}t_n + B_{13})}$$

4. Solution of the dynamic response of the saturated frozen soil foundation

4.1. Dynamic response of the foundation

The displacement component in the right angle coordinate system can be expressed by the potential functions φ and ψ

$$u_x = \frac{\partial \varphi}{\partial x} - \frac{\partial \psi}{\partial z} \qquad u_z = \frac{\partial \varphi}{\partial z} + \frac{\partial \psi}{\partial x} \tag{4.1}$$

Combining Eqs. (2.5) with Eq. (4.1), then substituting into Eqs. (2.4), the constitutive equation for the saturated frozen soil medium are be obtained as follows

$$\begin{aligned} \sigma_{zz}^S &= \Big(K_1 - \frac{2\mu_{11}}{3}\Big)\nabla^2\widetilde{\varphi}_S + C_{12}\nabla^2\widetilde{\varphi}_F + \Big(C_{13} - \frac{\mu_{13}}{3}\Big)\nabla^2\widetilde{\varphi}_I + 2\mu_{11}\Big(\frac{\partial^2\widetilde{\varphi}_S}{\partial z^2} + \frac{\partial^2\widetilde{\psi}_S}{\partial x \partial z}\Big) \\ &\quad + \mu_{13}\Big(\frac{\partial^2\widetilde{\varphi}_I}{\partial z^2} + \frac{\partial^2\widetilde{\psi}_I}{\partial x \partial z}\Big) \\ \sigma_{xz}^S &= \mu_{11}\Big(2\frac{\partial^2\widetilde{\varphi}_S}{\partial x \partial z} + \frac{\partial^2\widetilde{\psi}_S}{\partial x^2} - \frac{\partial^2\widetilde{\psi}_S}{\partial z^2}\Big) + \frac{1}{2}\mu_{13}\Big(2\frac{\partial^2\widetilde{\varphi}_I}{\partial x \partial z} + \frac{\partial^2\widetilde{\psi}_I}{\partial x^2} - \frac{\partial^2\widetilde{\psi}_I}{\partial z^2}\Big) \\ \sigma^F &= C_{12}\nabla^2\widetilde{\varphi}_S + K_2\nabla^2\widetilde{\varphi}_F + C_{23}\nabla^2\widetilde{\varphi}_I \\ \sigma_{zz}^I &= \Big(C_{13} - \frac{\mu_{13}}{3}\Big)\nabla^2\widetilde{\varphi}_S + C_{23}\nabla^2\widetilde{\varphi}_F + \Big(K_3 - \frac{2\mu_{33}}{3}\Big)\nabla^2\widetilde{\varphi}_I + \mu_{13}\Big(\frac{\partial^2\widetilde{\varphi}_S}{\partial z^2} + \frac{\partial^2\widetilde{\psi}_S}{\partial x \partial z}\Big) \\ &\quad + 2\mu_{33}\Big(\frac{\partial^2\widetilde{\varphi}_I}{\partial z^2} + \frac{\partial^2\widetilde{\psi}_I}{\partial x \partial z}\Big) \\ \sigma_{xz}^I &= \mu_{33}\Big(2\frac{\partial^2\widetilde{\varphi}_I}{\partial x \partial z} + \frac{\partial^2\widetilde{\psi}_I}{\partial x^2} - \frac{\partial^2\widetilde{\psi}_I}{\partial z^2}\Big) + \frac{1}{2}\mu_{13}\Big(2\frac{\partial^2\widetilde{\varphi}_S}{\partial x \partial z} + \frac{\partial^2\widetilde{\psi}_S}{\partial x^2} - \frac{\partial^2\widetilde{\psi}_S}{\partial z^2}\Big) \end{aligned} \tag{4.2}$$

Substituting Eqs. (3.7) and (3.13) into Eqs. (4.1) and (4.2) and combining the relationship between the parameters by Qiu *et al.* (2018), the expressions of displacement and stress of each phase in the saturated frozen soil medium in the Fourier transform domain can be obtained

$$
\begin{aligned}
\widetilde{u}_x^S &= i\xi \sum_{n=1}^{3}(D_n \mathrm{e}^{-\lambda_n z} + E_n \mathrm{e}^{\lambda_n z}) + \sum_{n=1}^{2} r_n (M_n \mathrm{e}^{-r_n z} - N_n \mathrm{e}^{r_n z}) \\
\widetilde{u}_z^S &= \sum_{n=1}^{3} -\lambda_n (D_n \mathrm{e}^{-\lambda_n z} - E_n \mathrm{e}^{\lambda_n z}) + \mathrm{i}\xi \sum_{n=1}^{2} (M_n \mathrm{e}^{-r_n z} + N_n \mathrm{e}^{r_n z}) \\
\widetilde{u}_z^F &= \sum_{n=1}^{3} -\lambda_n \delta_{pn}^F (D_n \mathrm{e}^{-\lambda_n z} - E_n \mathrm{e}^{\lambda_n z}) + \mathrm{i}\xi \sum_{n=1}^{2} \delta_{sn}^F (M_n \mathrm{e}^{-r_n z} + N_n \mathrm{e}^{r_n z}) \\
\widetilde{u}_x^I &= i\xi \sum_{n=1}^{3} \delta_{pn}^I (D_n \mathrm{e}^{-\lambda_n z} + E_n \mathrm{e}^{\lambda_n z}) + \sum_{n=1}^{2} r_n \delta_{sn}^I (M_n \mathrm{e}^{-r_n z} - N_n \mathrm{e}^{r_n z}) \\
\widetilde{u}_z^I &= \sum_{n=1}^{3} -\lambda_n \delta_{pn}^I (D_n \mathrm{e}^{-\lambda_n z} - E_n \mathrm{e}^{\lambda_n z}) + \mathrm{i}\xi \sum_{n=1}^{2} \delta_{sn}^I (M_n \mathrm{e}^{-r_n z} + N_n \mathrm{e}^{r_n z})
\end{aligned} \tag{4.3}
$$

and

$$
\begin{aligned}
\widetilde{\sigma}_{xz}^S &= \mathrm{i}\xi \sum_{n=1}^{3} -\lambda_n (2\mu_{11} + \mu_{13}\delta_{pn}^I)(D_n \mathrm{e}^{-\lambda_n z} - E_n \mathrm{e}^{\lambda_n z}) \\
&\quad - \sum_{n=1}^{2} (r_n^2 + \xi^2)\Big(\mu_{11} + \frac{1}{2}\mu_{13}\delta_{sn}^I]\Big)(M_n \mathrm{e}^{-r_n z} + N_n \mathrm{e}^{r_n z}) \\
\widetilde{\sigma}_{zz}^S &= \sum_{n=1}^{3} \chi_n (D_n \mathrm{e}^{-\lambda_n z} + E_n \mathrm{e}^{\lambda_n z}) - \mathrm{i}\xi \sum_{n=1}^{2} r_n (2\mu_{11} + \mu_{13}\delta_{sn}^I)(M_n \mathrm{e}^{-r_n z} - N_n \mathrm{e}^{r_n z}) \\
\widetilde{\sigma}_{zz}^F &= \sum_{n=1}^{3} (R_{12} + R_{22}\delta_{pn}^F + R_{23}\delta_{pn}^I)(\lambda_n^2 - \xi^2)(D_n \mathrm{e}^{-\lambda_n z} + E_n \mathrm{e}^{\lambda_n z}) \\
\widetilde{\sigma}_{xz}^I &= \mathrm{i}\xi \sum_{n=1}^{3} -\lambda_n (2\mu_{33}\delta_{pn}^I + \mu_{13})(D_n \mathrm{e}^{-\lambda_n z} - E_n \mathrm{e}^{\lambda_n z}) \\
&\quad - \sum_{n=1}^{2} (r_n^2 + \xi^2)\Big(\mu_{33}\delta_{sn}^I + \frac{1}{2}\mu_{13}\Big)(M_n \mathrm{e}^{-r_n z} + N_n \mathrm{e}^{r_n z}) \\
\widetilde{\sigma}_{zz}^I &= \sum_{n=1}^{3} \alpha_n (D_n \mathrm{e}^{-\lambda_n z} + E_n \mathrm{e}^{\lambda_n z}) - \mathrm{i}\xi \sum_{n=1}^{2} r_n (\mu_{13} + 2\mu_{33}\delta_{sn}^I)(M_n \mathrm{e}^{-r_n z} - N_n \mathrm{e}^{r_n z})
\end{aligned} \tag{4.4}
$$

where for $n = 1, 2, 3$

$$
\begin{aligned}
\chi_n &= [(R_{11} - 2\mu_{11}) + R_{12}\delta_{pn}^F + (R_{13} - \mu_{13})\delta_{pn}^I](\lambda_n^2 - \xi^2) + (2\mu_{11} + \mu_{13}\delta_{pn}^I)\lambda_n^2 \\
\alpha_n &= [(R_{13} - \mu_{13}) + R_{23}\delta_{pn}^F + (R_{33} - 2\mu_{33})\delta_{pn}^I](\lambda_n^2 - \xi^2) + (\mu_{13} + 2\mu_{33}\delta_{pn}^I)\lambda_n^2
\end{aligned}
$$

4.2. Boundary conditions and solution

Considering the boundary condition that the surface of foundation ($z = 0$) is permeable and subjected to a vertical harmonic load at $-l < x < l$, and the bottom surface of bedrock ($z = H$) is fixed and impermeable, we get:

— at $z = 0$

$$
\begin{aligned}
&\widetilde{\sigma}_{zz}^S + \widetilde{\sigma}_{zz}^F + \widetilde{\sigma}_{zz}^I = q_0 \frac{\sin \xi l}{\xi l} \qquad \widetilde{\sigma}_{xz}^S + \widetilde{\sigma}_{xz}^I = 0 \qquad \widetilde{\sigma}_{zz}^F = 0 \\
&\widetilde{u}_z^S = \widetilde{u}_z^I \qquad \widetilde{u}_x^S = \widetilde{u}_x^I
\end{aligned} \tag{4.5}
$$

— at $z = H$

$$
\widetilde{u}_x^S = 0 \qquad \widetilde{u}_z^S = 0 \qquad \widetilde{u}_z^F = 0 \qquad \widetilde{u}_x^I = 0 \qquad \widetilde{u}_z^I = 0 \tag{4.6}
$$

By substituting Eqs. (4.3) and (4.4) into Eqs. (4.5) and (4.6) boundary conditions, we obtain the following

$$\mathbf{Jx} = \mathbf{f} \tag{4.7}$$

where $\mathbf{J}$ is a 10×10 matrix, and

$$\mathbf{x} = [D_1, D_2, D_3, M_1, M_2, E_1, E_2, E_3, N_1, N_2]^{\mathrm{T}} \qquad \mathbf{f} = \left[q_0 \frac{\sin(\xi l)}{\xi l}, 0, 0, 0, 0, 0, 0, 0, 0, 0\right]^{\mathrm{T}}$$

By solving Eq. (4.7), $\mathbf{x}$ can be obtained. Combined with Eqs. (4.3) and (4.5), the stress and displacement of the saturated frozen soil foundation in the wavenumber domain can be found.

5. Numerical examples

In this Section, the effect of temperature T, porosity ϕ, cementation parameter ϖ, load frequency f, and contact parameter ε on the dynamic response is studied by numerical calculation when the boundary condition is permeable at the surface of the foundation and subjected to the vertical harmonic load, and the bottom is fixed and impermeable.

This paper chooses a collection of physical and mechanical parameters pertaining to the saturated frozen soil foundation, as illustrated in Table 1 (Qiu *et al.*, 2018). Take the load amplitude $q = 1\,\mathrm{kPa}$, saturated frozen soil thickness $H = 20\,\mathrm{m}$, distribution length $l = 1\,\mathrm{m}$. The closed-form solution of the inverse Fourier transform is challenging to obtain due to the intricate nature of the integrand function. Therefore, this paper employs the Fast Fourier Transform (FFT) method to perform the inverse Fourier transform. The wave number is discretized into 1024 points. The vertical and horizontal displacement examples in this paper take the calculation results at the surface of the foundation ($z = 0$)

Table 1. Physical and mechanical parameters of the saturated frozen soil foundation

Material parameters						
Hydrodynamic Viscosity coefficient	Density of soil particle	Density of liquid	Density of particles	Bulk modulus of soil particles	Bulk modulus of liquid	Bulk modulus of ice particle
η_F [Kg/(m s)]	ρ_s [Kg/m^3]	ρ_F [Kg/m^3]	ρ_I [Kg/m^3]	K_S [GPa]	K_F [GPa]	K_I [GPa]
$1.8 \cdot 10^{-3}$	2580	1000	920	20.9	2.25	8.58

Material parameters			
Shear modulus of soil particle	Shear modulus of ice particle	Reference value of soil skeleton permeability coeff.	Reference value of ice permeability coefficient
μ_S [GPa]	μ_I [GPa]	κ_{s0} [m^2]	κ_{i0} [m^2]
6.85	3.32	$1.0 \cdot 10^{-11}$	$5.0 \cdot 10^{-5}$

5.1. Verification

To verify the accuracy of the numerical calculations in this paper, the model is validated by degrading the Lamb problem in which the seismic source is located on the surface of a semi-infinite, single-phase homogeneous medium, and the results are compared with those of Yuan (1999) under the same conditions. A saturated permafrost foundation is degraded to an elastic

foundation when saturation $S_r \to 0$ and porosity $\phi \to 0$. Taking $\omega = 0.01\,\text{rad/s}$, Poisson's ratio $\nu = 0.3$, soil particle density $S_r = 1884\,\text{kg/m}^3$, and modulus of elasticity $E = 1 \cdot 10^7\,\text{Pa}$, Fig. 2 shows the variation of positive stress with depth under the load edge at the surface of the foundation where the bar load is applied. It can be seen that the vertical positive stresses in this paper are in good agreement with the results given by Yuan.

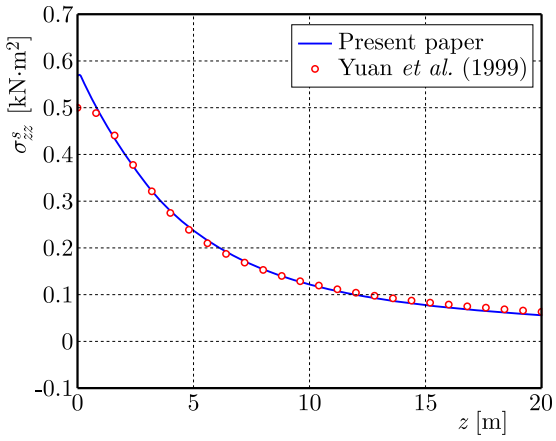

Fig. 2. The normal stress under the edge of the load when the strip load acts on the surface of the foundation

5.2. Effect of temperature

Changes in temperature cause changes in the composition of ice and liquid phases in saturated frozen soil, which in turn cause changes in the bearing capacity of the soil particle phase. Figures 3a and 3b show the effect curves of varying temperatures on the displacement of foundation under the condition of overburdened soil thickness $H = 20\,\text{m}$, porosity $\phi = 0.3$, Poisson's ratio $\nu = 0.3$, frequency $f = 1\,\text{Hz}$, and contact parameter $\varepsilon = 0.5$. As depicted in Figs. 3a

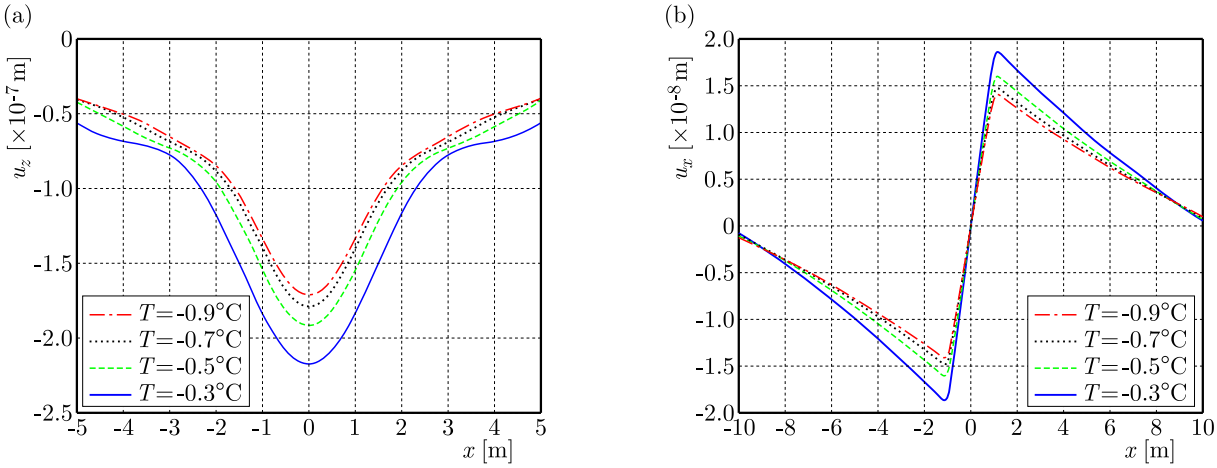

Fig. 3. Variation curves of the vertical and horizontal displacement of the foundation surface with temperature

and 3b, it becomes apparent that as the temperature rises, there is a noticeable escalation in both the magnitude of vertical and horizontal surface displacements. Furthermore, this increase in temperature leads to a gradual augmentation of the displacement amplitudes. This is because as the temperature increases, the ice particle content in the pore space gradually decreases, and the interaction with the soil particle skeleton gradually weakens so that the load borne by the

ice phase of the pore space decreases and the load borne by the soil particle phase increases, which finally makes the vertical displacement and horizontal displacement increase.

5.3. Effect of porosity

The ratio of the volume of connected pores in the unit body to the volume of unit body is the porosity, which is consistent with the actual geotechnical material, and the porosity is taken to be in the range of $\phi = 0.05$-0.50. The other parameters in the numerical calculation are selected as follows: $H = 20\,\mathrm{m}$, $T = -0.5^{\circ}\mathrm{C}$, $\nu = 0.3$, $f = 1\,\mathrm{Hz}$, $\varepsilon = 0.5$, ϕ taken as 0.1, 0.2, 0.3, 0.4, respectively. Figures 4a and 4b give the displacement curves of the saturated frozen soil foundation when the porosity is changed. From Figs. 4a and 4b, it is evident that variations in porosity exert a pronounced influence on both vertical and horizontal displacements of the foundation. Moreover, the displacements demonstrate an escalating trend with increasing porosity. This phenomenon can be attributed to the increase in porosity, which refers to the volume of interconnected pores within the unit body. As porosity increases, the volume of ice particles within the pores remains constant. Consequently, the supporting effect of ice particles on the soil particle framework gradually weakens. This causes an augmentation in the load carried by the soil particle framework, leading to a subsequent increase in the overall soil displacement.

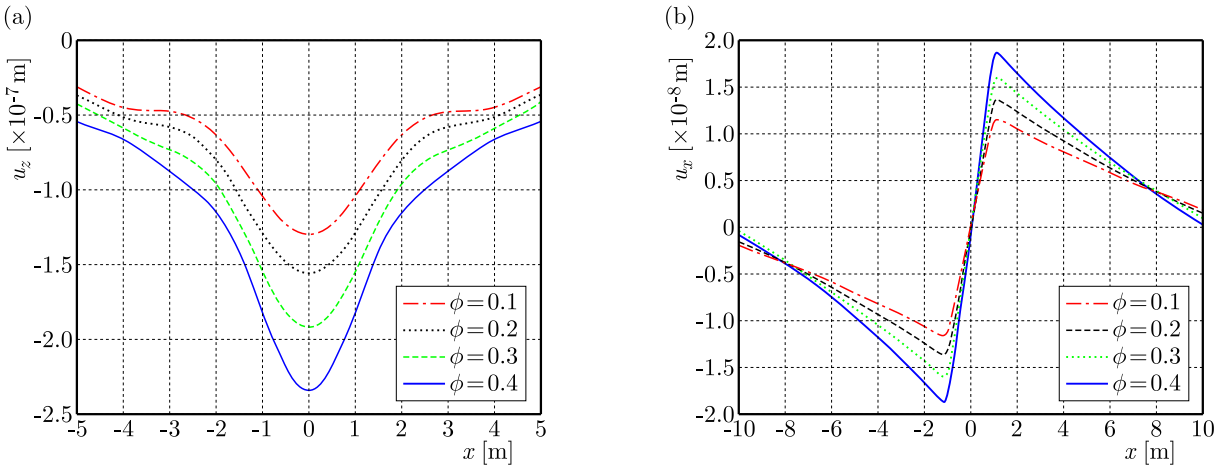

Fig. 4. Variation curves of the vertical and horizontal displacement of the foundation surface with porosity

5.4. Effect of cementation parameters

Imitating the relationship between modulus-porosity-Poisson's ratio of the two-phase medium and ignoring the effect of porosity on Poisson's ratio of the skeleton, Luo (1999) and Liu *et al.* (2015) believed that the cementation parameters can be taken as

$$\varpi = \frac{1+\nu}{2(1-2\nu)} \tag{5.1}$$

where ϖ denotes the level of overall cementation within the skeleton, ranging from 0.5 to infinity. A higher value of ϖ signifies a lower degree of cementation between particles, indicating a decreased bonding strength within the soil particle skeleton. ν denotes Poisson's ratio of the soil particle skeleton.

The range of Poisson's ratio considered in this study is $\nu = 0.100$ to 0.498, within which the cementation parameters exhibit an increasing trend with higher values of Poisson's ratio. Considering the overburdened thickness $H = 20\,\mathrm{m}$, temperature $T = -0.5^{\circ}\mathrm{C}$, porosity $\phi = 0.3$, load frequency $f = 1\,\mathrm{Hz}$, and contact parameter $\varepsilon = 0.5$, Figs. 5a and 5b present the curves of

displacement along the surface when Poisson's ratio ν gradually increases from 0.1 to 0.4, respectively. From these figures, it is evident that changes in Poisson's ratio, which corresponds to variations in the cementation parameter, have a significant impact on the amplitude of vertical and horizontal displacements of the ground surface. As Poisson's ratio increases (indicating an increase in the cementation parameter), both the vertical and horizontal displacements experience amplified amplitudes with the magnitude of displacement amplification gradually intensifying. This law can be explained as follows: an increase in the cementation parameters corresponds to a decrease in the degree of cementation between soil particles in saturated frozen soil and ice particles within the pores. This, in turn, results in a decrease in the skeleton modulus and softening of the soil. As a consequence, there is an increase in displacement observed.

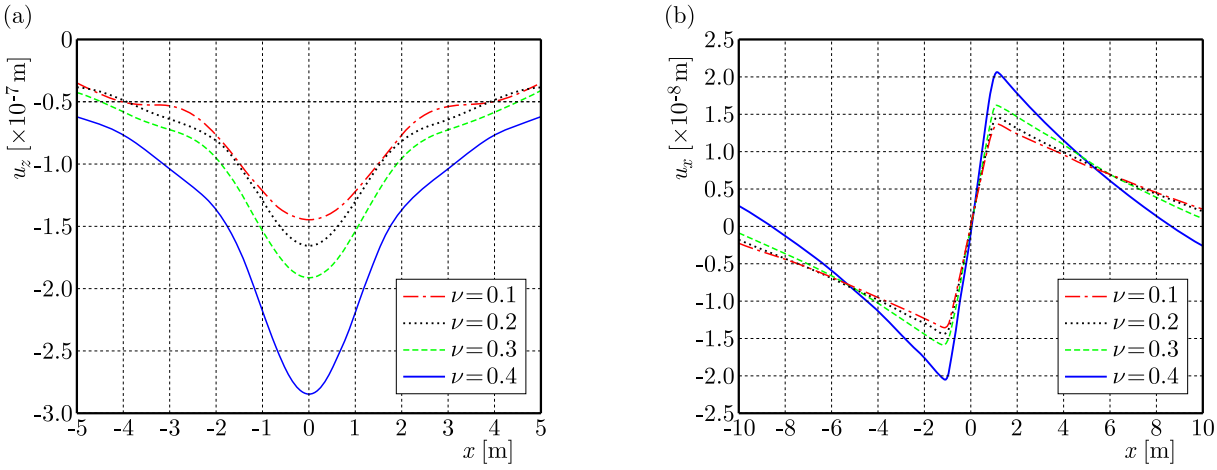

Fig. 5. Variation curves of the vertical and horizontal displacement of the foundation surface with cementation parameters

5.5. Effect of load frequency

Figures 6a and 6b analyze the influence of load frequency on the surface displacement of foundation. The following parameters are employed in the numerical calculations: overburden soil thickness $H = 20\,\text{m}$, temperature $T = -0.5°\text{C}$, Poisson's ratio $\nu = 0.3$, porosity $\phi = 0.3$, contact parameter $\varepsilon = 0.5$. The load frequencies considered are 1 Hz, 10 Hz, 20 Hz, and 30 Hz. From the observations made in Figs. 6a and 6b, it is apparent that as the load frequency increases, both the amplitude of vertical displacement and horizontal displacement of the ground surface also increase. This indicates that with an increase of load frequency, the load borne by the pore water and pore ice phases decreases, and the load borne by the soil particle phase increases.

5.6. Effect of contact parameters

The contact parameter ε characterizes the support of ice in the pore space on the skeleton of soil particles, and its value ranges from 0 to 1. When $\varepsilon = 1$, the ice has the smallest support to the soil particle skeleton, and the ice is suspended in the pores; when $\varepsilon = 0$, the ice has the largest support to the soil particle skeleton. The contact parameter affects the dynamic response of saturated permafrost foundation by influencing the bulk modulus K_{sm} and shear modulus μ_{sm} of the soil particles skeleton, which in turn affects the stiffness parameter. The relationship between the contact parameters and the volume and shear modulus of the skeletal mold of the soil particles is described in detail in Qiu *et al.* (2018). Figures 7a and 7b display the influence of contact parameters on the vertical and horizontal displacements of the surface under specific conditions: overlying soil layer thickness $H = 20\,\text{m}$, Poisson's ratio $\nu = 0.3$, temperature

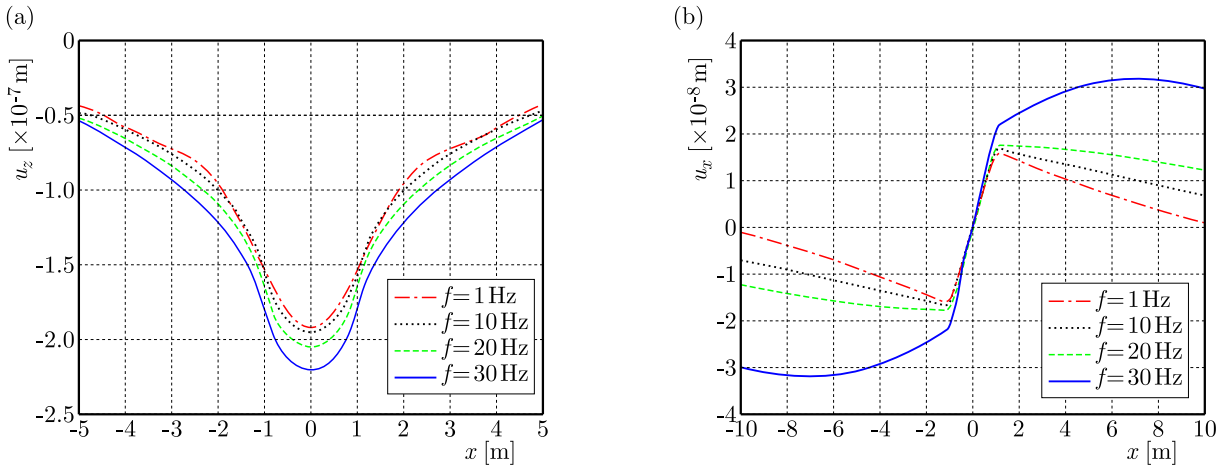

Fig. 6. Variation curves of the vertical and horizontal displacement of the foundation surface with load frequency

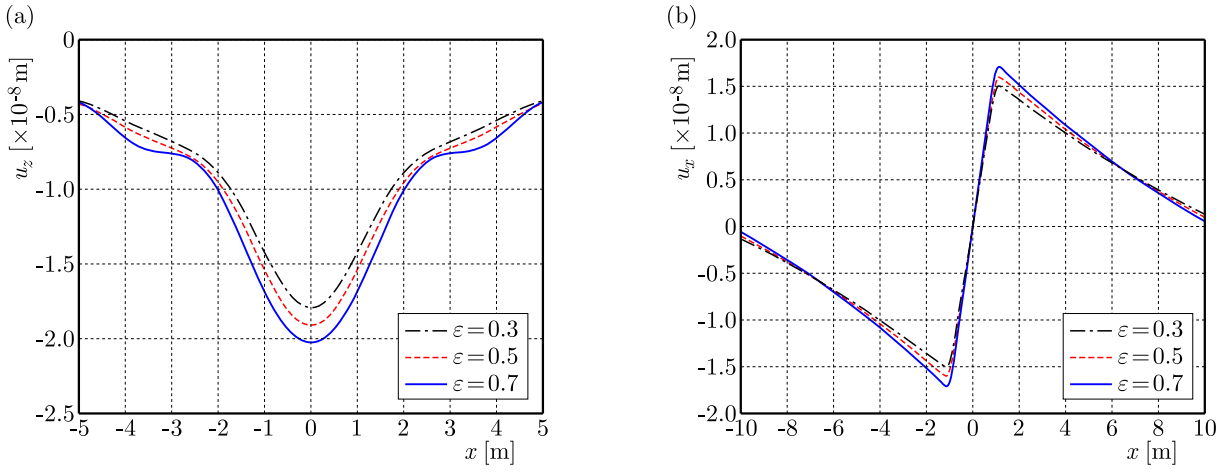

Fig. 7. Variation curves of the vertical and horizontal displacement of the foundation surface with contact parameters

$T = -0.5$°C, porosity $\phi = 0.3$, load frequency $f = 1$ Hz, and contact parameters $\varepsilon = 0.3$, 0.5, and 0.7. From Figs. 7a and 7b, it can be observed that an increase in the contact parameters leads to amplification in both the vertical and horizontal displacement amplitudes of the surface. This phenomenon can be attributed to the enlargement of pores between the ice particles and soil particle skeleton as the contact parameters increase. Consequently, there is a reduction in the friction force and an increase in the relative displacement between the ice and solid phases within the pores.

6. Conclusions

Based on the porous theory of porous solid medium, this paper establishes the governing equation of the two-dimensional dynamic response problem of a saturated frozen soil medium. Using the Fourier transform and boundary conditions, the solutions of the corresponding forces and displacements in the frequency domain of the saturated frozen soil foundation under the underlying bedrock under a harmonic load are obtained. Finally, the FFT method obtains the numerical results, and the influence of various parameters on the dynamic response of saturated frozen soil is analyzed in detail. The following conclusions are obtained:

- The amplitudes of vertical and horizontal displacements on the surface of saturated frozen soil foundations exhibit an increasing trend with elevated temperatures, porosity levels, cementation parameters, load frequencies, and contact parameters.
- The variations in porosity and cementation parameters within a saturated frozen soil foundation have a notable impact on the amplitude of both vertical and horizontal displacements.

Acknowledgments

The authors would like to express their gratitude to the National Natural Science Foundation of China (No. 52168053), the Qinghai Province Science and Technology Department Project (No. 2021-ZJ-922), and the China Postdoctoral Science Foundation (No. 2022MD723837) for their support. Additionally, the authors appreciate the insightful suggestions and comments provided by the reviewers.

References

1. Ai Z.Y., Mu J.J., Ren G.P., 2018, 3D dynamic response of a transversely isotropic multilayered medium subjected to a moving load, *International Journal for Numerical and Analytical Methods in Geomechanics*, **42**, 4, 636-654
2. Biot M.A., 1956, Theory of propagation of elastic waves in a fluid-saturated porous solid. II. Higher frequency range, *The Journal of the Acoustical Society of America*, **28**, 2, 179-191
3. Biot M.A., 1962, Mechanics of Deformation and Acoustic Propagation in Porous Media, *Journal of Applied Physics*, **33**, 4, 1482-1498
4. Carcione J.M., Gurevich B., Cavallini F., 2000, A generalized Biot-Gassmann model for the acoustic properties of shaley sandstones, *Geophysical Prospecting*, **48**, 3, 539-557
5. Carcione J.M., Santos J.E., Ravazzoli C.L., Helle H.B., 2003, Wave simulation in partially frozen porous media with fractal freezing conditions, *Journal of Applied Physics*, **94**, 12, 7839-7847
6. Carcione J.M., Seriani G., 2001, Wave simulation in frozen porous media, *Journal of Computational Physics*, **170**, 2, 676-695
7. Lamb H., 1904, On the Propagation of Tremors over the Surface of an Elastic Solid, *Philosophical Transactions of the Royal Society of London. Series A, Containing Papers of a Mathematical or Physical Character*, **203**, 359-371, 1-42
8. Leclaire P., Cohen-Ténoudji F., Aguirre-Puente J., 1994, Extension of Biot's theory of wave propagation to frozen porous media, *The Journal of the Acoustical Society of America*, **96**, 6, 3753-3768
9. Leclaire P., Cohen-Ténoudji F., Aguirre-Puente J., 1995, Observation of two longitudinal and two transverse waves in a frozen porous medium, *The Journal of the Acoustical Society of America*, **97**, 4, 2052-2055
10. Liang J., Wu M., Ba Z., Lee V.W., 2020, Transfer matrix solution to free-field response of a multi-layered transversely isotropic poroelastic half-plane, *Soil Dynamics and Earthquake Engineering*, **134**, 106168
11. Liu K., Zhang Z., Pan E., 2022, Dynamic response of a transversely isotropic and multilayered poroelastic medium subjected to a moving load, *Soil Dynamics and Earthquake Engineering*, **155**, 107154
12. Liu Z.J., 2015, Research on wave propagation characteristics and related problems in two-phase porous media, Ph.D. Thesis (in Chinese), Zhejiang University, China
13. Luo J., Stevens R., 1999, Porosity-dependence of elastic moduli and hardness of 3Y-TZP ceramics, *Ceramics International*, **25**, 3, 281-286

14. Ma Q., Huang Y.Y., Zhou F.X., 2023, Dynamic response study of layered unsaturated foundation under moving load based on TRM method (in Chinese), *Engineering Mechanics*, 1-11

15. Ma Q., Shi L.W., 2022, Dynamic response of two-dimensional double-layered unsaturated soil foundations under a strip load, *Journal of Vibration Engineering and Technologies*, **10**, 4, 1221-1233

16. Ma W., Wang X., Wang B., Zhou S., Leong E.-C., Wang C., 2023, Three-dimensional axisymmetric transient response of an unsaturated poroelastic transversely isotropic half-space, *Computers and Geotechnics*, **159**, 105482

17. Qiu H.M., Xia T.D., Zheng Q.Q., Zhou F., 2018, Parametric studies of body wave propagation in saturated frozen soil (in Chinese), *Rock and Soil Mechanics*, **39**, 4053-4062

18. Shi L.W., Ma Q., Ma Y., 2021, Dynamic responses of unsaturated half-space soils to a strip load at different boundary conditions, *Arabian Journal of Geosciences*, **14**, 947

19. Xu M.J., 2010, *Investigation on Dynamic Response of Unsaturated Soils and Foundation* (in Chinese), South China University of Technology, China

20. Xu M.J., Wei D.M., 2011, 3D non-axisymmetrical dynamic response of unsaturated soils (in Chinese), *Engineering Mechanics*, **28**, 3, 78-85

21. Xu M.Q., Jin L.H., Li J.H., 2009, Dynamic responses of a layered saturated soil subjected to harmonic horizontal loads (in Chinese), *Rock and Soil Mechanics*, **30**, 9, 536-540

22. Yuan J.Y., Zhao X.H., 1999, Formulas for calculating stresses in soil subjecting to vertical line load and strip distributed load beneath the surface of ground (in Chinese), *Chinese Quarterly of Mechanics*, **2**, 156-165

23. Zhou B., 2020, Study on ground motion and Rayleigh wave propagation characteristics in frozen soil area, Master's Thesis (in Chinese), Zhejiang Ocean University, China

24. Zhou F.X., Lai Y.M., 2011, Propagation characteristics of elastic waves in saturated frozen soil (in Chinese), *Rock and Soil Mechanics*, **32**, 2669-2674

25. Zhou F.X., Lai Y.M., Ren Y.Y., 2013, An analysis on saturated soil foundation under harmonic loads (in Chinese). *Chinese Journal of Solid Mechanics*, **34**, 5, 536-540

Manuscript received July 20, 2023; accepted for print April 25, 2024